

# $p$ -wave superconductivity induced from valley symmetry breaking in twisted trilayer graphene

J. González<sup>1</sup> and T. Stauber<sup>2</sup>

<sup>1</sup> Instituto de Estructura de la Materia, CSIC, E-28006 Madrid, Spain

<sup>2</sup> Materials Science Factory, Instituto de Ciencia de Materiales de Madrid, CSIC, E-28049 Madrid, Spain

(Dated: September 29, 2024)

We show that the  $e$ - $e$  interaction induces a strong breakdown of valley symmetry in twisted trilayer graphene, just before the superconducting instability develops in the hole-doped material. We analyze this effect in the framework of an atomistic self-consistent Hartree-Fock approximation, which is a sensible approach as the Fock part becomes crucial to capture the dynamical breakdown of symmetry. This effect allows us to reproduce the experimental observation of the Hall density, including the reset at 2-hole doping. Furthermore, the breakdown of valley symmetry has important consequences for the superconductivity, as it implies a reduction of symmetry down to the  $C_3$  group which operates in a single valley. We observe that the second valence band has a three-fold van Hove singularity, which is pinned to the Fermi level at the experimental optimal doping for superconductivity. We further find that the  $C_3$  configuration of the saddle points leads to a version of Kohn-Luttinger superconductivity where the dominant pairing amplitude has  $p$ -wave symmetry. We stress that the breakdown of symmetry down to  $C_3$  may be shared by other materials with valley symmetry breaking in the strong correlation regime, so that it may be an essential ingredient to capture the right order parameter of the superconductivity in those systems, especially when this relies on a purely electronic mechanism of pairing driven by the strongly anisotropic  $e$ - $e$  scattering.

*Introduction.*— The discovery of superconductivity and its parent insulating phases at the magic angle of twisted bilayer graphene (TBG)<sup>1,2</sup> has opened a new era in the investigation of strongly correlated phenomena in two-dimensional electron systems. There is an ongoing debate about the origin of the superconductivity in TBG<sup>3–33</sup>, which could also clarify whether a similar phenomenon can arise in other moiré van der Waals materials. In this regard, superconductivity has been already observed in twisted trilayer graphene (TTG),<sup>34,35</sup> showing unconventional features like reentrant behavior under large magnetic fields.<sup>36–39</sup>

Apart from the superconductivity, another remarkable effect in TBG is the observation of symmetry breaking at integer fillings of the lowest valence and conduction bands.<sup>40–42</sup> This effect is most evident in the recurrent reset of the Fermi level to a sequence of Dirac points as the lowest valence (conduction) bands are emptied (filled), which points at the complete splitting of valley and spin degenerate bands.<sup>43</sup>

TTG has also shown a striking phenomenon of reset of the Hall density at integer fillings of the lowest valence and conduction bands.<sup>34,35</sup> Especially at 2-hole doping, it has been found that the Hall density jumps from a divergent value down to zero. This observation is particularly important, since the effect of reset precedes the development of the superconducting regime right below 2-hole doping (as well as right above 2-electron doping in the conduction band). This feature of Hall density reset may be used then as a source of valuable information about the effects of the electronic interaction.

In this paper, we show that the extended Coulomb interaction has a natural tendency to induce the breakdown of the valley symmetry of TTG. This effect becomes very strong at 2-hole doping, in such a way that, above a cer-

tain interaction strength, a gap opens up between the empty first valence band (VB) and the occupied second VB. The top of the second VB has quadratic dispersion, but the empty first VB develops an extremely flat shape, with the alignment of the van Hove singularity to the bottom of the band. We show that this different behavior of the two bands is at the origin of the experimentally observed reset of the Hall density.

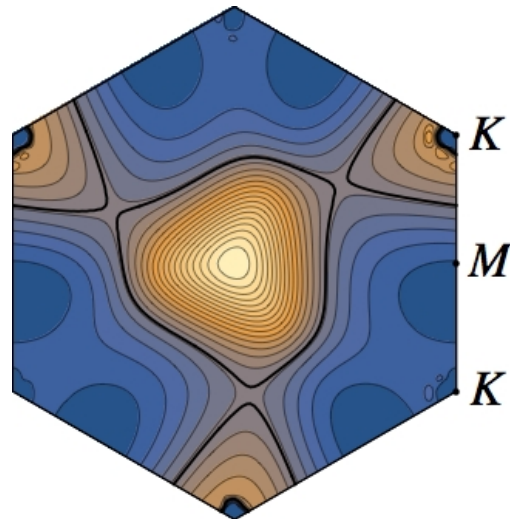


FIG. 1. Energy contour map of the second valence band in the Brillouin zone of TTG at twist angle  $\theta \approx 1.61^\circ$ , for dielectric constant  $\epsilon = 24$  of the Coulomb interaction and filling fraction of 2.4 holes per moiré unit cell. The thick contour stands for the Fermi line. Contiguous contour lines differ by a constant step of 0.4 meV, from lower energies in blue to higher energies in light color.

The breakdown of valley symmetry leads to a strong

distortion of the first and second VBs. The rotational symmetry of the bands is actually reduced from  $C_6$  to  $C_3$ , as the latter is the symmetry enforced in a single valley. A plot of the second VB in the regime of valley symmetry breaking is shown in Fig. 1, for a filling fraction of 2.4 holes per moiré unit cell.

The reduction of rotational symmetry has profound implications for the superconductivity, as the order parameter must be consistent with the  $C_3$  modulation of the dispersion. As shown in Fig. 1, the second VB has a three-fold van Hove singularity, which remains very close to the Fermi level about the experimental optimal doping of 2.4 holes per moiré unit cell.<sup>44</sup> This leads to a strong angular modulation of the  $e$ - $e$  scattering, which is the condition needed to induce a so-called Kohn-Luttinger (pairing) instability, driven solely by the electron interaction. We have found that the  $C_3$  configuration of the saddle points leads in general to a dominant pairing amplitude in the  $\{\cos(\phi), \sin(\phi)\}$  representation, consistent with the spin-triplet superconductivity which is likely observed in the experiments. This reflects the deep connection between valley symmetry breaking and unconventional superconductivity, both developing as a result of the strong interaction effects.

We stress that the breakdown of symmetry down to  $C_3$  may be shared by other two-valley electron systems in the strong correlation regime such as TBG or rhombohedral trilayer graphene. This may be therefore an essential ingredient to understand properly the superconductivity in those systems, especially when it relies on a purely electronic mechanism of pairing triggered by the strongly anisotropic  $e$ - $e$  scattering.

*Valley symmetry breaking.*— We deal with the setup of TTG usually realized in the experiments, in which the two outer layers are rotated by the same angle  $\theta$  with respect to the central layer. We model this configuration by taking a twist angle  $\theta \approx 1.61^\circ$  belonging to the set of commensurate superlattices realized by TBG. Then, the low-energy states are distributed into a Dirac-like band, with states even under mirror symmetry with respect to the central plane, and two additional valence and conduction bands, with states odd under the mirror symmetry (see the Appendix). The latter are the counterpart of the lowest-energy bands of TBG, and they become progressively flatter when approaching the magic angle of TTG, which is  $\approx 1.6^\circ$ .

In what follows, we apply a fully atomistic approach to TTG, based on a tight-binding model for the  $\pi$  orbitals of the carbon atoms. The Hamiltonian  $H$  can be written as the sum

$$H = H_0 + H_{\text{int}} , \quad (1)$$

where  $H_0$  represents the non-interacting tight-binding Hamiltonian and  $H_{\text{int}}$  is the interaction part. This can be expressed in terms of creation (annihilation) operators  $a_{i\sigma}^\dagger$  ( $a_{i\sigma}$ ) for electrons at each carbon site  $i$  with spin  $\sigma$

as

$$H_{\text{int}} = \frac{1}{2} \sum_{i,j,\sigma,\sigma'} a_{i\sigma}^\dagger a_{i\sigma} v_{\sigma\sigma'}(\mathbf{r}_i - \mathbf{r}_j) a_{j\sigma'}^\dagger a_{j\sigma'} , \quad (2)$$

We take  $v_{\sigma\sigma'}$  as the extended Coulomb potential, with the long-range tail cut off at a distance dictated by the screening length  $\xi$ , arising from the presence of nearby metallic gates, and with the strength further reduced by the dielectric constant  $\epsilon$  accounting for the dielectric environment (see the Appendix for all the details).

We resort to a self-consistent Hartree-Fock approximation in order to study the effects of the  $e$ - $e$  interaction. In this approach, the full electron propagator  $G$  is represented in terms of a set of eigenvalues  $\varepsilon_{a\sigma}$  and eigenvectors  $\phi_{a\sigma}(\mathbf{r}_i)$  modified by the interaction, in such a way that in the static limit

$$(G)_{i\sigma,j\sigma} = - \sum_a \frac{1}{\varepsilon_{a\sigma}} \phi_{a\sigma}(\mathbf{r}_i) \phi_{a\sigma}(\mathbf{r}_j)^* . \quad (3)$$

In the Hartree-Fock approximation, the electron self-energy  $\Sigma$  can be also expressed entirely in terms of the set of  $\phi_{a\sigma}(\mathbf{r}_i)$ . In the static limit, we have

$$\begin{aligned} (\Sigma)_{i\sigma,j\sigma} = & 2\mathbb{I}_{ij} \sum_a' \sum_{l,\sigma'} v_{\sigma\sigma'}(\mathbf{r}_i - \mathbf{r}_l) |\phi_{a\sigma'}(\mathbf{r}_l)|^2 \\ & - v_{\sigma\sigma}(\mathbf{r}_i - \mathbf{r}_j) \sum_a' \phi_{a\sigma}(\mathbf{r}_i) \phi_{a\sigma}(\mathbf{r}_j)^* , \end{aligned} \quad (4)$$

where the prime means that the sum is to be carried over the occupied levels<sup>45</sup>.

The Fock contribution to the self-energy (4) becomes essential in order to account for the breakdown of the valley symmetry. This is characterized in our approach by the development of a nonvanishing condensate

$$S_\sigma = \text{Im} \left( \sum_{i \in A} \left( h_{i_1 i_2}^{(\sigma)} h_{i_2 i_3}^{(\sigma)} h_{i_3 i_1}^{(\sigma)} \right)^{\frac{1}{3}} - \sum_{i \in B} \left( h_{i_1 i_2}^{(\sigma)} h_{i_2 i_3}^{(\sigma)} h_{i_3 i_1}^{(\sigma)} \right)^{\frac{1}{3}} \right) \quad (5)$$

where the sums run over the loops made of three nearest neighbors  $i_1, i_2$  and  $i_3$  of each atom  $i$  in graphene sublattices  $A$  and  $B$ , with matrix elements

$$h_{ij}^{(\sigma)} = \sum_a' \phi_{a\sigma}(\mathbf{r}_i) \phi_{a\sigma}(\mathbf{r}_j)^* . \quad (6)$$

In the continuum theory of Dirac fermions, the condensate (5) translates into the generation of a term proportional to the identity in pseudospin space. This does not open a gap in the Dirac cones at the  $K$  point, but instead it leads to a different shift in the energy of the cones in the two valleys of the electron system, with the consequent valley symmetry breaking.

In the non-interacting picture, the two lowest VBs are very close in energy and actually degenerate along the  $\Gamma K$  and  $KM$  directions, as a result of the superposition

of the two graphene valleys in the Brillouin zone of TTG. However, we find that this degeneracy is appreciably lost for values of the dielectric constant  $\epsilon \lesssim 70$ . This can be seen in Fig. 2, which shows the low-energy bands of TTG at a filling fraction corresponding to 2-hole doping. We observe that, for dielectric constant  $\epsilon = 24$ , a gap as large as  $\approx 4$  meV opens up between the empty first VB and the occupied second VB.

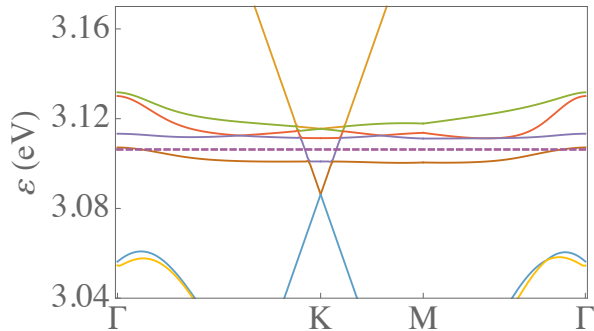


FIG. 2. Lowest valence and conduction bands of TTG at twist angle  $\theta \approx 1.61^\circ$ , computed in a self-consistent Hartree-Fock approximation with dielectric constant  $\epsilon = 24$  and filling fraction of 2 holes per moiré unit cell (the dashed line stands for the Fermi level).

As a consequence of the valley symmetry breaking, the two lowest VBs become very different, as can be seen in Fig. 3. From this figure, also the reduction of symmetry of the bands down to the  $C_3$  group becomes evident. All these features leave their fingerprint in experimental observations, as we discuss in what follows.

*Hall density reset.*— Experimentally, a reset from a large value down to zero Hall density is observed in TTG at the filling fraction of 2-hole doping (as well as at 2-electron doping in the conduction side). In our interacting model, we can explain such a discontinuity as a result of the jump of the Fermi level across the gap shown in Fig. 2, from the bottom of the first VB to the top of the second VB.

As shown in the Appendix, in the semiclassical approximation, general closed trajectories usually lead to a universal Hall density  $n_H = n$ . Even extreme elliptic trajectories still fall under this universality class and anharmonic effects usually only lead to slight deviations. We thus start from a symmetric band model for each valence band where half of the band is dominated by electron transport and the other half by hole transport.

Strong deviations from  $n_H = n$  only come from open trajectories which are usually linked to van Hove singularities. Around these points, the diverging Hall density is given by

$$n_H = \frac{n}{\pi} \ln \frac{\alpha \Lambda^2}{|\mu| + k_B T}, \quad (7)$$

where  $\alpha$  is a band parameter,  $\Lambda$  the phenomenological

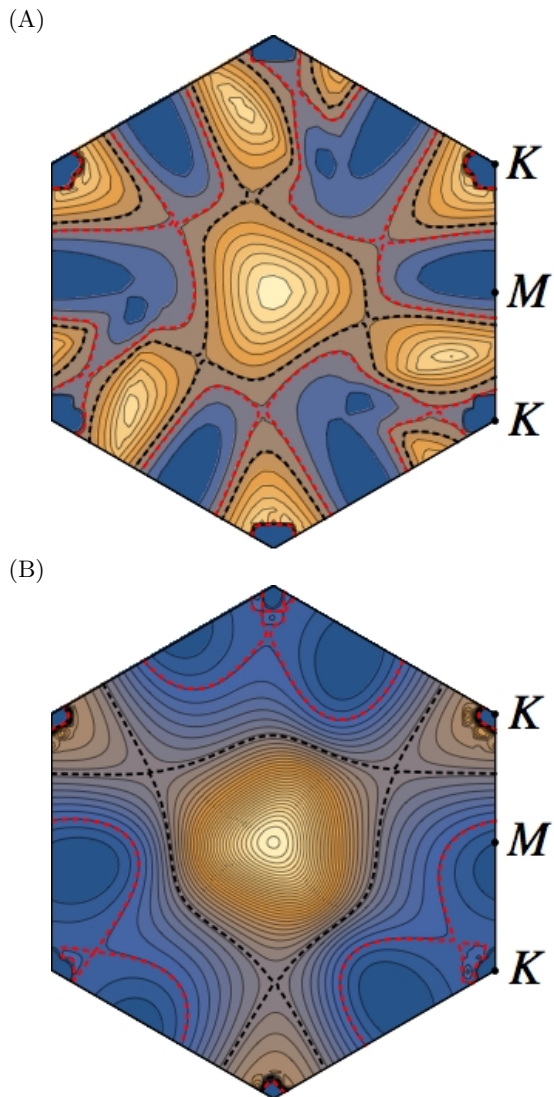


FIG. 3. Energy contour maps of the first (A) and the second VB (B) in the Brillouin zone of TTG at twist angle  $\theta \approx 1.61^\circ$ , for dielectric constant  $\epsilon = 24$  of the Coulomb interaction and filling fraction of 2 holes per moiré unit cell. Contiguous contour lines differ by a constant step of 0.2 meV, from lower energies in blue to higher energies in light color. The contours at the two van Hove singularities are indicated in black and red.

band-cutoff and  $\mu$  the corresponding relative chemical potential related to the electronic density  $n$ . We also introduce the finite temperature  $T$  that smears out the logarithmic divergency. Details on the derivation of Eq. (7) and the fitting procedure are given in the Appendix.

For a quantitative discussion of the Hall density in TTG, we consider the first and second VBs for  $n = -2$ , shown in Fig. 3. We expect deviations due to different filling factors to only shift the energy of the van Hove singularity corrections, which is related to the observed pinning of the chemical potential to the van Hove singularity. Due to the pronounced gap between the first

and the second VB, there is a reset of the Hall density at  $n = -2$ . Moreover, we find  $n_H = n$  around half-filling due to the closed orbits of the band structure. This is also the case around filling factors  $n = 0$  and  $n = -4$ .

Both VBs are characterized by the appearance of two van Hove singularities that occur at certain filling factors of the bands, see Fig. 3. Around these energies, the Fermi lines lead to open trajectories in the semiclassical description and the deviation of the universal result will be modeled by Eq. (7). Fig. 4 shows the Hall density  $n_H$  as function of the electronic density  $n$  for different temperatures  $T = 0, 1, 10$  K. The energies and respective filling factors of the van Hove singularities are indicated by the logarithmic divergence for  $T = 0$ , that should slightly move when the doping dependent band structure is taken into account. We remark that the curve for  $T = 1$  K agrees well with the plot for vanishing displacement field in Fig. 6c of the Extended Data of Ref. 34, which is a good validation of our approach.

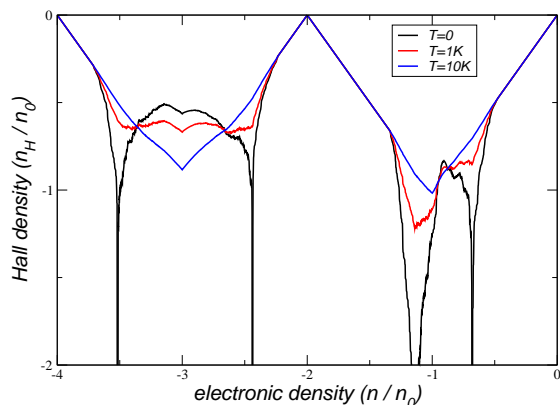


FIG. 4. Hall density as function of the electronic density in units of the density of one electron in the moiré supercell  $n_0$  for three temperatures  $T = 0, 1, 10$  K. The reset at  $n = -2$  emerges due to the gap at the half-filled valence band, see Fig. 2. The deviations from the universal behavior due to the presence of van Hove singularities is described by Eq. (7). The contours at the van Hove singularities of each band are indicated in black and red in Fig. 3.

*p-wave superconductivity.*— The  $e$ - $e$  interaction can give rise to a pairing instability when the anisotropy of the electron scattering is strong enough to induce attraction in a given pairing channel. This is typically reflected as a negative coupling in the expansion of the Cooper pair vertex  $V$  in the different harmonics  $\cos(n\phi)$ ,  $\sin(n\phi)$ .

The vertex  $V$  is indeed a function of the angles  $\phi$  and  $\phi'$  of the respective momenta of the spin-up incoming and outgoing electrons on each contour line of energy  $\varepsilon$ . The scattering of Cooper pairs in the particle-particle channel leads to a reduction of the amplitude of the vertex, given

by the equation

$$V(\phi, \phi') = V_0(\phi, \phi') - \frac{1}{(2\pi)^2} \int^{\Lambda_0} \frac{d\varepsilon}{\varepsilon} \int_0^{2\pi} d\phi'' \frac{\partial k_{\perp}}{\partial \varepsilon} \frac{\partial k_{\parallel}}{\partial \phi''} V_0(\phi, \phi'') V(\phi'', \phi') \quad (8)$$

where  $k_{\parallel}, k_{\perp}$  are the respective longitudinal and transverse components of the momentum for each energy contour line while  $V_0(\phi, \phi')$  is the bare vertex at an energy cutoff  $\Lambda_0$ . The origin of the BCS instability can be seen by differentiating Eq. (8) with respect to the cutoff  $\Lambda_0$ , which leads to

$$\varepsilon \frac{\partial \widehat{V}(\phi, \phi')}{\partial \varepsilon} = \frac{1}{2\pi} \int_0^{2\pi} d\phi'' \widehat{V}(\phi, \phi'') \widehat{V}(\phi'', \phi') \quad (9)$$

after redefining  $\widehat{V}(\phi, \phi') = F(\phi)F(\phi')V(\phi, \phi')$  with  $F(\phi) = \sqrt{(\partial k_{\perp}/\partial \varepsilon)(\partial k_{\parallel}/\partial \phi)/2\pi}$ . Then, when there is a negative eigenvalue of  $\widehat{V}$  in the expansion of the harmonics, Eq. (9) leads to a divergent flow for that particular eigenvalue as  $\varepsilon \rightarrow 0$ . This is the signature of the pairing instability as the Fermi line is approached in the low-energy limit.

The crucial point is the determination of  $V_0(\phi, \phi')$  at a sensible value of the cutoff  $\Lambda_0$ , for which one usually takes an effective theory of low-energy electron quasiparticles with interactions already screened at the scale  $\Lambda_0$ . Assuming for simplicity that the effective interaction is averaged to a Hubbard repulsion  $U$  over each moiré unit cell, the relevant scattering processes (as identified in the original work by Kohn and Luttinger) can be summed up in the particle-hole channel to give

$$V_0(\phi, \phi') = U + \frac{U^2 \chi_{\mathbf{k}+\mathbf{k}'}}{1 - U \chi_{\mathbf{k}+\mathbf{k}'}} + \frac{U^3 \chi_{\mathbf{k}-\mathbf{k}'}}{1 - U^2 \chi_{\mathbf{k}-\mathbf{k}'}} \quad (10)$$

where  $\mathbf{k}, \mathbf{k}'$  are the respective momenta at angles  $\phi, \phi'$  and  $\chi_{\mathbf{q}}$  is the particle-hole susceptibility at momentum transfer  $\mathbf{q}$ .

When evaluating  $V_0(\phi, \phi')$  for a band like that in Fig. 1, the vertex has a natural expansion in terms of irreducible representations of the approximate symmetry  $C_{3v}$ . These can be characterized in terms of Fourier components, so that we have  $A_1 \rightarrow \{\cos(3n\phi)\}$ ,  $A_2 \rightarrow \{\sin(3n\phi)\}$  for integer  $n$ , and  $E \rightarrow \{\cos(m\phi), \sin(m\phi)\}$  for  $m \neq 3n$ . We find that there is in general a dominant pairing instability characterized by a negative coupling for the degenerate terms  $\cos(\phi), \sin(\phi)$  in the expansion of  $V_0(\phi, \phi')$ . Besides, another negative coupling appears but with smaller magnitude for the harmonic  $\cos(3\phi)$ . The couplings with largest magnitude in the expansion of the vertex can be seen in Table I, for the particular case of Hubbard repulsion  $U/a_M^2 = 2.7$  meV ( $a_M$  being the moiré lattice constant of TTG) and filling fraction of 2.4 holes per moiré unit cell.

*Conclusion.*— We have shown that the  $e$ - $e$  interaction induces a strong breakdown of valley symmetry in TTG, just before the superconducting instability develops in the hole-doped material. We have analyzed this effect in

Eigenvalue $\lambda$	harmonics	Irr. Rep.
0.75	$\{\cos(2\phi), \sin(2\phi)\}$	E
0.34	$\{\cos(4\phi), \sin(4\phi)\}$	E
-0.23	$\{\cos(\phi), \sin(\phi)\}$	E
0.21	$\cos(6\phi)$	$A_1$
0.17	$\sin(6\phi)$	$A_2$
-0.15	$\cos(3\phi)$	$A_1$
0.09	$\{\cos(8\phi), \sin(8\phi)\}$	E
-0.05	$\sin(3\phi)$	$A_2$

TABLE I. Eigenvalues of the Cooper-pair vertex with largest magnitude (not including the constant mode) and their respective irreducible representations of the approximate  $C_{3v}$  symmetry for  $U/a_M^2 = 2.7$  meV and filling fraction of 2.4 holes per moiré unit cell.

the framework of a self-consistent Hartree-Fock approximation, which is a sensible approach as the Fock part becomes crucial to capture the dynamical breakdown of symmetry. This feature is validated in our model as it allows us to reproduce the experimental observation of the Hall density reset at 2-hole doping. This reset arises naturally in our approach from the large gap that opens up between the first and the second VB at that filling level.

The breakdown of valley symmetry has important consequences for the superconductivity of TTG, as it implies

a reduction of symmetry down to the  $C_3$  rotational group which operates in each single valley. This means that the anisotropy of the electron scattering is greatly enhanced, making possible a Kohn-Luttinger mechanism of superconductivity where the order parameter is prone to  $p$ -wave symmetry. We also expect the superconducting order parameter to have lifted spin degeneracy.<sup>46</sup>

Valley symmetry breaking seems to be an ubiquitous feature in many moiré systems, and it is plausible that its role in the development of superconductivity may be also important in other derivatives of graphene. In this regard, it is remarkable that superconductivity (possibly in a spin-triplet channel) has been recently found in rhombohedral trilayer graphene, which is another system close to an isospin instability. It would be pertinent then to reexamine the superconductivity in such systems, including TBG, to confirm the connection between valley symmetry breaking and  $p$ -wave pairing put forward in this paper.

*Acknowledgements.* This work has been supported by MINECO (Spain) under Grant No. FIS2017-82260-P, MICINN (Spain) under Grant No. PID2020-113164GB-I00, as well as by the CSIC Research Platform on Quantum Technologies PTI-001. The access to computational resources of CESGA (Centro de Supercomputación de Galicia) is also gratefully acknowledged.

## APPENDIX

### I. TIGHT-BINDING APPROACH AND HARTREE-FOCK APPROXIMATION FOR TWISTED TRILAYER GRAPHENE

We model twisted trilayer graphene in a tight-binding approach, taking as starting point the non-interacting Hamiltonian:

$$H_0 = - \sum_{\langle i,j \rangle} t_{\parallel}(\mathbf{r}_i - \mathbf{r}_j) (a_{i\sigma}^\dagger a_{j\sigma} + h.c.) - \sum_{(i,j)} t_{\perp}(\mathbf{r}_i - \mathbf{r}_j) (a_{i\sigma}^\dagger a_{j\sigma} + h.c.), \quad (11)$$

The sum over the brackets  $\langle \dots \rangle$  runs over pairs of atoms in the same layer, whereas the sum over the curved brackets  $(\dots)$  runs over pairs with atoms belonging to different layers (1 to 3).  $t_{\parallel}(\mathbf{r})$  and  $t_{\perp}(\mathbf{r})$  are hopping matrix elements which have an exponential decay with the distance  $|\mathbf{r}|$  between carbon atoms. A common parametrization is based on the Slater-Koster formula for the transfer integral<sup>47</sup>

$$-t(\mathbf{d}) = V_{pp\pi}(d) \left[ 1 - \left( \frac{\mathbf{d} \cdot \mathbf{e}_z}{d} \right)^2 \right] + V_{pp\sigma}(d) \left( \frac{\mathbf{d} \cdot \mathbf{e}_z}{d} \right)^2 \quad (12)$$

with

$$V_{pp\pi}(d) = V_{pp\pi}^0 \exp\left(-\frac{d-a_0}{r_0}\right), V_{pp\sigma}(d) = V_{pp\sigma}^0 \exp\left(-\frac{d-d_0}{r_0}\right), \quad (13)$$

where  $\mathbf{d}$  is the vector connecting the two sites,  $\mathbf{e}_z$  is the unit vector in the  $z$ -direction,  $a_0$  is the C-C distance and  $d_0$  is the distance between layers. A typical choice of parameters is given by  $V_{pp\pi}^0 = -2.7$  eV,  $V_{pp\sigma}^0 = 0.48$  eV and  $r_0 = 0.319a_0$ <sup>47</sup>. In practice, we have taken these values to carry out the analysis reported in the main text, but restricting within each layer the hopping to nearest-neighbor atoms, as a way to get closer to the magic angle condition.

At the twist angles considered in the paper, the in-plane lattice relaxation of twisted trilayer graphene does not have the important role that it plays at the magic angle of the twisted bilayer. However, the out-of-plane corrugation

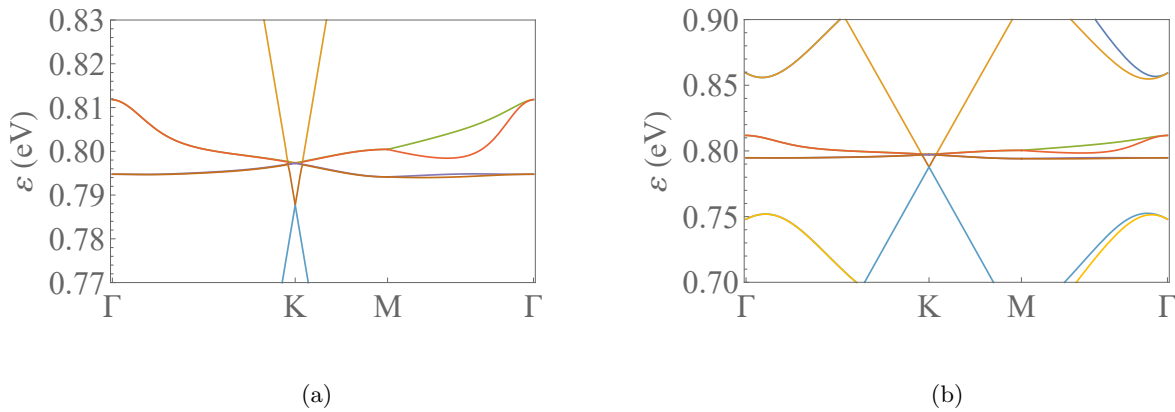


FIG. 5. Dispersion of the first valence and conduction bands (zoomed out in (b)) about the charge neutrality point of twisted trilayer graphene with twist angle  $\theta \approx 1.61^\circ$ , computed in a tight-binding approach with parameters given in the text.

of the trilayer is a relevant effect, which arises from the dependence of the interlayer interaction on the stacking of the graphene layers. Thus, the lattice structure tends to relax in the out-of-plane direction, reaching a minimum interlayer distance in the regions of *AB* stacking, and a maximum value in the regions of *AA* stacking. To describe the interlayer interaction we have used a Kolmogorov-Crespi potential<sup>48,49</sup>

$$U(z) = -A \left( \frac{z_0}{z} \right)^6 + C e^{-\lambda(z-z_0)} \quad (14)$$

where the first term stands for the van der Waals attraction and the second term accounts for an exponentially decaying repulsion due to the interlayer wave-function overlap. The effect of the registry of the carbon atoms is included in the second term, and we have adjusted it to interpolate between the different interaction energies in the regions of *AB* and *AA* stacking. In the relaxed structure we have left the central layer intact, so that the separation of the outer layers about the center becomes modulated across the superlattice according to the potential (14), reaching a minimum interlayer distance of 0.334 nm for *AB* stacking and a maximum distance of 0.356 nm for *AA* stacking.

Overall, our tight-binding approach leads to sensible results for the commensurate lattice studied in the main text with twist angle  $\theta \approx 1.61^\circ$ , whose first valence and conduction bands are shown in Fig. 5.

Turning to the *e-e* interaction, we have considered a form of the Coulomb potential which is adapted to the case where twisted trilayer graphene is surrounded by top and bottom metallic gates. The starting point is the unscreened Coulomb potential  $v_0(\mathbf{r}) = e^2/4\pi\epsilon r$ ,  $\epsilon$  being the dielectric constant of the surrounding (non-metallic) medium. In the presence of a gate at distance  $z = \xi/2$ , the electrostatic energy of two electrons lying in a plane parallel to the electric gate and being separated by a distance  $r$  is given by

$$v(\mathbf{r}) = \frac{e^2}{4\pi\epsilon} \left( \frac{1}{r} - \frac{1}{\sqrt{r^2 + \xi^2}} \right). \quad (15)$$

In the presence of an additional opposite gate also at distance  $z = \xi/2$ , and again using the image-charge technique, one obtains for the electrostatic energy

$$v(\mathbf{r}) = \frac{e^2}{4\pi\epsilon} \sum_{n=-\infty}^{\infty} \frac{(-1)^n}{\sqrt{r^2 + n^2 \xi^2}} \quad (16)$$

$$= \frac{e^2}{4\pi\epsilon} \frac{2\sqrt{2} e^{-\pi r/\xi}}{\xi \sqrt{r/\xi}}. \quad (17)$$

In the main text, we have addressed in particular the case of a setup with  $\xi = 10$  nm.

When implementing the Hartree-Fock approximation, the construction of the self-energy in Eq. (4) of the main text demands the knowledge of the eigenvectors of the Hamiltonian. That self-energy implies a sum over the occupied states of the electronic bands, but in practice one has to impose some kind of truncation when carrying out the calculation. In this respect, we have retained the first 51 valence bands in the self-consistent resolution. Moreover, we have computed the self-energy taking a grid with 192 momenta (plus the Gamma point) covering the Brillouin zone. We have checked that such a content of filled states is safe to capture the relevant symmetry-breaking patterns of twisted trilayer graphene, as well as to obtain a sensible description of its low-energy bands.

## II. SEMICLASSICAL THEORY OF THE HALL DENSITY

In this Section, we will summarize known results for the Hall density within the semiclassical theory. We will then also outline the derivation of the Hall density around a general van Hove singularity.

We start the discussion with the Chamber's formula

$$\sigma_{ij} = \frac{g_s g_v e^2}{(2\pi)^2} \int d^2 k v_i(\mathbf{k}) \int_{-\infty}^0 dt' v_j(\mathbf{k}(t')) e^{t'/\tau} \left( -\frac{\partial f(E)}{\partial E} \right). \quad (18)$$

By virtue of the Lorentz force rule, this can be transformed in the following expression:<sup>50</sup>

$$\sigma_{ij} = \frac{g_s g_v e^3 B}{(2\pi)^2 \hbar^2} \int_0^T dt v_i(t) \int_{-\infty}^t dt' v_j(t') e^{(t'-t)/\tau} \quad (19)$$

Limiting the dynamics of an electron to one band, the time evolution for the position and the wave vector is given by the following two semiclassical equations:

$$\dot{\mathbf{r}} = \mathbf{v}(\mathbf{k}) = \frac{1}{\hbar} \partial_{\mathbf{k}} \epsilon_{\mathbf{k}} \quad (20)$$

$$\dot{\mathbf{k}} = -\frac{e}{\hbar} [\mathbf{E} + \mathbf{v}(\mathbf{k}) \times \mathbf{B}] \quad (21)$$

We assume the magnetic field perpendicular to the plane and the electric field in  $x$ -direction, i.e.,  $\mathbf{B} = B\mathbf{e}_z$  and  $\mathbf{E} = E\mathbf{e}_x$ . The equations of motion in the plane can be integrated and yield

$$\mathbf{r}(t) = -\frac{\hbar}{eB} \mathbf{e}_z \times \mathbf{k}(t) - \frac{E}{B} \mathbf{e}_y t. \quad (22)$$

The drift velocity  $\mathbf{v}_D = -\frac{E}{B} \mathbf{e}_y$  is in fact the velocity of the frame of reference in which the electric field vanishes.<sup>51</sup> We can thus combine the equations of motion to the following compact form where only the magnetic field appears:

$$\dot{\mathbf{k}} = -\frac{e}{\hbar^2} \partial_{\mathbf{k}} \tilde{\epsilon}_{\mathbf{k}} \times \mathbf{B}, \quad (23)$$

with  $\tilde{\epsilon}_{\mathbf{k}} = \epsilon_{\mathbf{k}} - \hbar \mathbf{k} \cdot \mathbf{v}_D$ .

Generally, the trajectory in  $\mathbf{k}$ -space can be split into a closed and open orbit. The closed orbit is periodic in  $T$  and can be expanded into a Fourier transform. The effect of an open orbit can be modelled by an average drift velocity  $\mathbf{v}^o$ . This gives for the two components  $i = x, y$

$$k_i(t) = \sum_{\nu} \kappa_{\nu}^i e^{i\nu\omega_c t} + v_i^o t. \quad (24)$$

We could also introduce a modulation via a periodic function with  $\delta k^o(0) = \delta k^o(T) = 0$ , but we expect no qualitative differences. In our simple assumption, there are thus no cross-terms between closed and open orbits and we can discuss both contributions separately.

### A. Closed orbits

For closed orbits, we get with the notation of Eq. (24)

$$\sigma^c = \frac{g_s g_v e^2 \tau}{2\pi m_c} \sum_{\nu > 0} \frac{\nu^2}{1 + (\nu\omega_c \tau)^2} \left( -\operatorname{Re} \left[ \frac{|\kappa_{\nu}^y|^2}{\kappa_{\nu}^x \kappa_{-\nu}^y (1 - i\nu\omega_c \tau)} \right] - \operatorname{Re} \left[ \frac{\kappa_{\nu}^x \kappa_{-\nu}^y (1 + i\nu\omega_c \tau)}{|\kappa_{\nu}^x|^2} \right] \right). \quad (25)$$

Since  $\kappa_{\nu}^x$  is independent of  $B$ , this generally proves the Onsager relation  $\sigma_{xy}(B) = \sigma_{yx}(-B)$ . To be more explicit, we will now discuss isotropic and elliptic models.

For the general isotropic dispersion  $\epsilon_{\mathbf{k}} = \alpha |k|^{\xi}$  and for  $k_F = (\mu/\alpha)^{1/\xi}$ , we have  $k_x = k_F \cos(\omega_c t)$  and  $k_y = k_F \sin(\omega_c t)$  with the cyclotron frequency  $\omega_c = \frac{eB}{m_c}$  and  $m_c = \frac{\hbar^2}{\xi \alpha} k_F^{2-\xi}$ . This yields the same result as the general definition

$m_c = \frac{\hbar^2}{2\pi} \frac{\partial A}{\partial \mu}$  with  $A = \pi k_F^2$  denoting the area that is enclosed by the cyclotron orbit. With  $(g_s g_v / 4) k_F^2 = \pi n$ , where  $g_s$  and  $g_v$  denote spin and valley (or other) degeneracies, this then gives the well-known result

$$\sigma = \frac{\sigma_{xx}}{1+a^2} \begin{pmatrix} 1 & a \\ -a & 1 \end{pmatrix}, \quad (26)$$

where the longitudinal conductivity is given by  $\sigma_{xx} = e^2 n \tau / m_c$  and  $a = \omega_c \tau$ . With the resistivity tensor  $\rho = \sigma^{-1}$ , we get for all isotropic dispersion relations the universal Hall density

$$n_H = - \left[ e \frac{d\rho_{xy}}{dB} \right]^{-1} = n. \quad (27)$$

The universal result also holds for an elliptic dispersion with  $\epsilon_{\mathbf{k}} = \alpha_x k_x^2 + \alpha_y k_y^2$  and  $k_{F,i} = \sqrt{\mu / \alpha_i}$ . With  $k_x = k_{F,x} \cos(\omega_c t)$ ,  $k_y = k_{F,y} \sin(\omega_c t)$ ,  $A = \pi k_{F,x} k_{F,y}$  and  $\omega_c = \frac{eB}{m_c}$ , we have  $m_c = \frac{\hbar^2}{2\sqrt{\alpha_x \alpha_y}}$  and

$$\sigma = \frac{\sigma_{xx}}{1+a^2} \begin{pmatrix} \sqrt{\alpha_x / \alpha_y} & a \\ -a & \sqrt{\alpha_y / \alpha_x} \end{pmatrix}, \quad (28)$$

where  $\sigma_{xx} = \frac{e^2 n \tau}{m_c}$ . We, therefore, get again for the Hall density the universal expression  $n_H = n$  independent of the band parameters.

For trigonal warped Fermi-surfaces, there are deviations from the universal result. However, in a perturbative treatment the first non-vanishing term is quadratic in the expansion parameter. This suggests that general closed orbits will lead to a Hall density close to the universal result, i.e.,  $n = n_H$ .

## B. Open orbits

Let us now consider open orbits. The position at  $t = 0$  after the mean time  $\tau$  after the last collision is given by

$$\frac{\mathbf{r}(0) - \mathbf{r}(-\tau)}{\tau} = -\frac{\hbar}{eB} \mathbf{e}_z \times \frac{(\mathbf{k}(0) - \mathbf{k}(-T))}{T} + \mathbf{v}_D \quad (29)$$

where we assumed that  $\tau/T$  cycles have been performed with period  $T = 2\pi/\omega_c$  and cyclotron frequency  $\omega_c = \frac{eB}{m_c}$ . As argued above, we can set  $\mathbf{v}_D = 0$ . With  $\mathbf{n} = -\mathbf{e}_z \times \mathbf{n}_{\mathbf{k}}$ , we thus obtain for the mean velocity

$$\mathbf{v}^o = \frac{\hbar}{m_c b} \mathbf{n}, \quad (30)$$

where we set  $\mathbf{k}(0) - \mathbf{k}(-T) = \frac{2\pi}{b} \mathbf{n}_{\mathbf{k}}$  with  $b$  the dimension of the quadratic unit cell.

Since there are open orbits in both directions, the net contribution turns out to be zero. However, an applied electric field will populate the states in one direction more than the other direction and we will get a net current in the direction  $\mathbf{n}$  that can be written as

$$\mathbf{j} = \sigma^o \mathbf{n} (\mathbf{n} \cdot \mathbf{E}) + \sigma^c \mathbf{E}, \quad (31)$$

where  $\sigma^{o/c}$  stems from open/closed circuits. We have  $\sigma^o \rightarrow \text{const}$  and  $\sigma^c \rightarrow 0$  for  $B \rightarrow \infty$ .

For open orbits, we find

$$\sigma^o = \frac{g_s g_v}{2\pi} \frac{e^2 \tau}{m_c} \mathbf{v}^o \mathbf{v}^o, \quad (32)$$

with  $\mathbf{v}^o$  defined in Eq. (30) which leads to Eq. (31).

Following the discussion of Ashcroft and Mermin,<sup>51</sup> we then obtain for the magnetoresistance

$$\rho = \frac{(\mathbf{n}_{\mathbf{k}} \cdot \mathbf{j})^2}{\mathbf{n}_{\mathbf{k}} \cdot \sigma^c \cdot \mathbf{n}_{\mathbf{k}}}. \quad (33)$$

This quantity diverges in the high-field limit. There are thus deviations from the universal result for open orbits which emerge around van Hove singularities in the band structure.



### C. Trajectories close to van Hove singularities

To discuss the semiclassical motion of electrons close to a van Hove singularities, a well-defined regularization procedure is needed since the orbits are unbounded for a continuum theory. For this, we will not use the Chamber's formula, but start from the macroscopic equations of motion for the current density. The general response theory in the presence of an in-plane electric field  $\mathbf{E}$  and a perpendicular magnetic field  $\mathbf{B}$  then reads

$$\partial_t \mathbf{j} = \chi \mathbf{E} + \frac{e}{m_c} \bar{\mathbf{j}} \times \mathbf{B} - \eta \mathbf{j}. \quad (34)$$

Above, we introduced the current-current response function  $\chi$  in the dc-limit defined and the "average" current density  $\bar{\mathbf{j}}$  to be discussed below.

The so-called Drude response can be entirely obtained from the band structure and for  $T = 0$ , this can be written as

$$\chi_{ij} = \frac{g_s g_v e^2}{(2\pi \hbar)^2} \int d^2 k (\nabla \epsilon_{\mathbf{k}})_i (\nabla \epsilon_{\mathbf{k}})_j \delta(\mu - \epsilon_{\mathbf{k}}). \quad (35)$$

By choosing the principle axes, we can always assume  $\chi$  to be diagonal. We also introduced the inverse relaxation time  $\eta = \tau^{-1}$  and the cyclotron mass is defined by<sup>51</sup>

$$m_c = \frac{\hbar^2}{2\pi} \frac{\partial A}{\partial \mu}, \quad (36)$$

where  $A$  denotes the area that is enclosed by the cyclotron orbit. Within this formalism, the above results for the isotropic and elliptic models can be obtained. Here, we will outline the specific case of a hyperbolic model.

For a van Hove singularity with  $\epsilon_{\mathbf{k}} = -\alpha_- k_x^2 + \alpha_+ k_y^2$ , the angular integration is eliminated by the  $\delta$ -function. For the evaluation of the second integral, the following integrals are needed:

$$\mathcal{I}_{\pm}(\Lambda, \gamma) = \int_1^{\Lambda^2} dx \sqrt{\frac{x-1}{\gamma x+1}}^{\pm 1} \quad (37)$$

This gives for  $\mu = \pm|\mu|$  the final expression

$$\chi_{\pm} = \frac{g_s g_v e^2}{(2\pi)^2 \hbar^2} \frac{4\tilde{\mu}_{\pm}}{(\alpha_+ + \alpha_-)} \begin{pmatrix} \alpha_-^2 \mathcal{I}_{\pm}(\tilde{\Lambda}_{\pm}, \gamma_{\pm}) & 0 \\ 0 & \alpha_+^2 \mathcal{I}_{\mp}(\tilde{\Lambda}_{\pm}, \gamma_{\pm}) \end{pmatrix}, \quad (38)$$

with  $\gamma_{\pm} = \alpha_{\mp}/\alpha_{\pm}$ ,  $\tilde{\mu}_{\pm} = |\mu|/\alpha_{\pm}$ , and  $\tilde{\Lambda}_{\pm} = \Lambda/\sqrt{\tilde{\mu}_{\pm}}$  where  $\Lambda$  denotes the wavenumber cutoff. In the following, we will only discuss the response due to electron doping with  $\mu > 0$  and set  $\gamma = \gamma_+$ .

At the neutrality point, the susceptibility is proportional to  $\Lambda^2$  and we will discuss the difference  $\delta\chi = \chi_+ - \chi_{\mu=0}$ . To leading order, we have

$$\delta\chi = \frac{g_s g_v e^2}{(2\pi)^2 \hbar^2} 2\mu \begin{pmatrix} -\sqrt{\gamma} \ln \frac{\alpha \Lambda^2}{\mu} & 0 \\ 0 & \sqrt{\gamma}^{-1} \ln \frac{\alpha \Lambda^2}{\mu} \end{pmatrix}, \quad (39)$$

where  $\alpha = \frac{2\alpha_+\alpha_-}{\alpha_+\alpha_-}$ . The area relative to the one of  $\mu = 0$  is given by  $A = 4 \frac{\mu}{\sqrt{\alpha_+\alpha_-}} \ln \frac{4\alpha_-\Lambda^2}{\mu}$ . Therefore, we have in leading order  $m_c = 4 \frac{\hbar^2}{2\pi\sqrt{\alpha_+\alpha_-}} \ln \frac{4\alpha_-\Lambda^2}{\mu}$ . With  $n = \frac{g_s g_v}{(2\pi)^2} A$ , this yields

$$\frac{m_c}{e^2} \delta\chi = \frac{n}{\pi} \begin{pmatrix} -\sqrt{\gamma} \ln \frac{\alpha \Lambda^2}{\mu} & 0 \\ 0 & \sqrt{\gamma}^{-1} \ln \frac{\alpha \Lambda^2}{\mu} \end{pmatrix}. \quad (40)$$

Let us now include the magnetic field. A magnetic field does not break rotational invariance and for an anisotropic system, the field couples to the average velocity  $v^2 = v_x v_y$ . For an elliptic dispersion, this yields the universal results  $n_H = n$  as mentioned above.

However, in the case of a saddle-point, we also have to keep track of the negative sign and we have to couple to the positive mean velocity  $v^2 = -v_x v_y$ . From the velocity  $v_i = \hbar^{-1} \partial_{k_i} \epsilon_{\mathbf{k}}$  and  $\mathbf{j} = -en\mathbf{v}$ , we thus set  $\bar{\mathbf{j}} = (j_x/\sqrt{\gamma}, -\sqrt{\gamma}j_y)$ . The hyperbolic response with respect to  $\mu = 0$  gives then rise to the following conductivity tensor:

$$\sigma = \frac{\tau}{1-a^2} \begin{pmatrix} \delta\chi_1 & -a\sqrt{\gamma}\delta\chi_2 \\ -a\delta\chi_1/\sqrt{\gamma} & \delta\chi_2 \end{pmatrix}, \quad (41)$$

$\epsilon_{vH}$	$n_{vH}$	$\alpha_-$	$\alpha_+$	$\alpha$	$\Lambda$
3.11041	0.68	3.95	1.52	2.20	1.05
3.11020	1.14	1.52	9.12	2.61	0.38
3.11020	1.14	1.06	0.70	0.84	0.68
3.10088	2.43	1.33	1.52	1.42	2.15
3.09959	3.51	6.08	6.08	6.08	0.62

TABLE II. Energy of the van Hove singularities  $\epsilon_{vH}$  (in eV), the corresponding filling number  $n_{vH}$ , and the fitting parameters  $\alpha_{\pm}$  in units of  $\text{meV}a_M^2$  defining the saddle point dispersion  $\epsilon_{\mathbf{k}} = -\alpha_-k_1^2 + \alpha_+k_2^2$ . We also list the scale that enters the expression of the Hall density,  $\alpha = \frac{2\alpha_+ + \alpha_-}{\alpha_+ + \alpha_-}$  (in  $\text{meV}a_M^2$ ), and the band cutoff  $\Lambda$  (in  $a_M^{-1}$ ).

where we used  $\delta\chi = \text{diag}(\delta\chi_1, \delta\chi_2)$  of Eq. (39). The resistivity tensor thus reads

$$\rho = \frac{\eta}{\delta\chi_1\delta\chi_2} \begin{pmatrix} \delta\chi_2 & a\sqrt{\gamma}\delta\chi_2 \\ a\delta\chi_1/\sqrt{\gamma} & \delta\chi_1 \end{pmatrix}. \quad (42)$$

Therefore, we get for the Hall density the final result

$$n_H = - \left[ e \frac{d\rho_{xy}}{dB} \right]^{-1} = \frac{n}{\pi} \ln \frac{\alpha\Lambda^2}{\mu}. \quad (43)$$

There is a logarithmic divergence for  $\mu \rightarrow 0$  which has been discussed also in the context of a tight-binding model.<sup>50</sup> However, for extended van Hove singularities there is also a possible divergency in the limit  $\alpha \rightarrow 0$  which is independent of  $\mu$ .

### III. FITTING OF VAN HOVE SINGULARITIES

We start from a symmetric transport model, i.e., half of the band is dominated by electron transport and the other half by hole transport. This "universal behavior" is modified by the presence of two van Hove singularities which shall be modeled by Eq. (43). This expression depends on the parameters  $\alpha$  and  $\Lambda$  which shall now be determined.

Before we outlined the fitting procedure, let us recall that there is a prominent valley symmetry breaking which reduces the inherent  $C_6$ -symmetry to a  $C_3$ -symmetry. This symmetry is also reflected in the van Hove singularities which always composed of saddle-points that come in triplets. Interestingly, at filling factor  $n = -1.14$ , there are two saddle-point triplets. These shall be discussed separately.

Due to numerical errors, the  $C_3$ -symmetry regarding the three-fold saddle points is not exact even though the appearance in the density plot of Fig. 3 of the main text suggests this approximate symmetry. We thus chose to fit the saddle point along the principle axis by the general dispersion  $\epsilon_{\mathbf{k}} = -\alpha_-k_1^2 + \alpha_+k_2^2$  which is closest to a parabola with positive and negative mass. The results are listed in Table II.

We determine the band-cut off by demanding continuity with the universal regime  $n_H = n$  at the cross-over chemical potential  $\mu^*$  corresponding to the filling factor  $n^*$ :

$$\Lambda^2 = \frac{\mu^*}{\alpha} e^{\pi} \quad (44)$$

For the crossover density  $|n^* - n_{vH}| = \Delta n$ , we set  $\Delta n = 0.2$ . For doping levels between two of the van Hove singularities, i.e., in the range  $|n_{vH,1} - n_{vH,2}| - 2\Delta n$ , we choose a linear interpolation of the two logarithmic singularities. Finite temperature effects are included by substituting  $|\mu| \rightarrow |\mu| + k_B T$  that smears out the logarithmic singularity.

<sup>1</sup> Y. Cao, V. Fatemi, A. Demir, S. Fang, S. L. Tomarken, J. Y. Luo, J. D. Sanchez-Yamagishi, K. Watanabe, T. Taniguchi, E. Kaxiras, R. C. Ashoori, and P. Jarillo-Herrero, Nature **556**, 80 EP (2018).

<sup>2</sup> Y. Cao, V. Fatemi, S. Fang, K. Watanabe, T. Taniguchi, E. Kaxiras, and P. Jarillo-Herrero, Nature **556**, 43 EP (2018).

<sup>3</sup> C. Xu and L. Balents, Phys. Rev. Lett. **121**, 087001 (2018).

<sup>4</sup> G. E. Volovik, JETP Letters **107**, 516 (2018).

<sup>5</sup> N. F. Q. Yuan and L. Fu, Phys. Rev. B **98**, 045103 (2018).

<sup>6</sup> H. C. Po, L. Zou, T. Senthil, and A. Vishwanath, Phys. Rev. B **99**, 195455 (2019).

- <sup>7</sup> B. Roy and V. Jurivčić, Phys. Rev. B **99**, 121407 (2019).
- <sup>8</sup> H. Guo, X. Zhu, S. Feng, and R. T. Scalettar, Phys. Rev. B **97**, 235453 (2018).
- <sup>9</sup> J. F. Dodaro, S. A. Kivelson, Y. Schattner, X. Q. Sun, and C. Wang, Phys. Rev. B **98**, 075154 (2018).
- <sup>10</sup> G. Baskaran, arXiv:1804.00627.
- <sup>11</sup> C.-C. Liu, L.-D. Zhang, W.-Q. Chen, and F. Yang, Phys. Rev. Lett. **121**, 217001 (2018).
- <sup>12</sup> K. Slagle and Y. B. Kim, SciPost Phys. **6**, 16 (2019).
- <sup>13</sup> T. J. Peltonen, R. Ojajärvi, and T. T. Heikkilä, Phys. Rev. B **98**, 220504 (2018).
- <sup>14</sup> D. M. Kennes, J. Lischner, and C. Karrasch, Phys. Rev. B **98**, 241407 (2018).
- <sup>15</sup> M. Koshino, N. F. Q. Yuan, T. Koretsune, M. Ochi, K. Kuroki, and L. Fu, Phys. Rev. X **8**, 031087 (2018).
- <sup>16</sup> J. Kang and O. Vafek, Phys. Rev. X **8**, 031088 (2018).
- <sup>17</sup> H. Isobe, N. F. Q. Yuan, and L. Fu, Phys. Rev. X **8**, 041041 (2018).
- <sup>18</sup> Y.-Z. You and A. Vishwanath, arXiv:1805.06867.
- <sup>19</sup> F. Wu, A. H. MacDonald, and I. Martin, Phys. Rev. Lett. **121**, 257001 (2018).
- <sup>20</sup> Y.-H. Zhang, D. Mao, Y. Cao, P. Jarillo-Herrero, and T. Senthil, Phys. Rev. B **99**, 075127 (2019).
- <sup>21</sup> M. Ochi, M. Koshino, and K. Kuroki, Phys. Rev. B **98**, 081102 (2018).
- <sup>22</sup> A. Thomson, S. Chatterjee, S. Sachdev, and M. S. Scheurer, Phys. Rev. B **98**, 075109 (2018).
- <sup>23</sup> S. Carr, S. Fang, P. Jarillo-Herrero, and E. Kaxiras, Phys. Rev. B **98**, 085144 (2018).
- <sup>24</sup> F. Guinea and N. R. Walet, Proceedings of the National Academy of Sciences **115**, 13174 (2018).
- <sup>25</sup> L. Zou, H. C. Po, A. Vishwanath, and T. Senthil, Phys. Rev. B **98**, 085435 (2018).
- <sup>26</sup> J. González and T. Stauber, Phys. Rev. Lett. **122**, 026801 (2019).
- <sup>27</sup> M. Yankowitz, S. Chen, H. Polshyn, Y. Zhang, K. Watanabe, T. Taniguchi, D. Graf, A. F. Young, and C. R. Dean, Science **363**, 1059 (2019).
- <sup>28</sup> Y. Choi, J. Kemmer, Y. Peng, A. Thomson, H. Arora, R. Polski, Y. Zhang, H. Ren, J. Alicea, G. Refael, F. von Oppen, K. Watanabe, T. Taniguchi, and S. Nadj-Perge, Nature Physics **15**, 1174 (2019).
- <sup>29</sup> A. L. Sharpe, E. J. Fox, A. W. Barnard, J. Finney, K. Watanabe, T. Taniguchi, M. A. Kastner, and D. Goldhaber-Gordon, Science **365**, 605 (2019).
- <sup>30</sup> S. Moriyama, Y. Morita, K. Komatsu, K. Endo, T. Iwasaki, S. Nakaharai, Y. Noguchi, Y. Wakayama, E. Watanabe, D. Tsuya, K. Watanabe, and T. Taniguchi, arXiv:1901.09356.
- <sup>31</sup> Y. Jiang, X. Lai, K. Watanabe, T. Taniguchi, K. Haule, J. Mao, and E. Y. Andrei, Nature **573**, 91 (2019).
- <sup>32</sup> Y. Xie, B. Lian, B. Jäck, X. Liu, C.-L. Chiu, K. Watanabe, T. Taniguchi, B. A. Bernevig, and A. Yazdani, Nature **572**, 101 (2019).
- <sup>33</sup> A. Kerelsky, L. J. McGilly, D. M. Kennes, L. Xian, M. Yankowitz, S. Chen, K. Watanabe, T. Taniguchi, J. Hone, C. Dean, A. Rubio, and A. N. Pasupathy, Nature **572**, 95 (2019).
- <sup>34</sup> J. M. Park, Y. Cao, K. Watanabe, T. Taniguchi, and P. Jarillo-Herrero, Nature **590**, 249 (2021).
- <sup>35</sup> Z. Hao, A. M. Zimmerman, P. Ledwith, E. Khalaf, D. H. Najafabadi, K. Watanabe, T. Taniguchi, A. Vishwanath, and P. Kim, Science **371**, 1133 (2021).
- <sup>36</sup> E. Khalaf, A. J. Kruchkov, G. Tarnopolsky, and A. Vishwanath, Phys. Rev. B **100**, 085109 (2019).
- <sup>37</sup> S. Carr, C. Li, Z. Zhu, E. Kaxiras, S. Sachdev, and A. Kruchkov, Nano Letters **20**, 3030 (2020).
- <sup>38</sup> A. Lopez-Bezanilla and J. L. Lado, Phys. Rev. Research **2**, 033357 (2020).
- <sup>39</sup> A. Fischer, Z. A. H. Goodwin, A. A. Mostofi, J. Lischner, D. M. Kennes, and L. Klebl, arXiv:2104.10176.
- <sup>40</sup> U. Zondiner, A. Rozen, D. Rodan-Legrain, Y. Cao, R. Queiroz, T. Taniguchi, K. Watanabe, Y. Oreg, F. von Oppen, A. Stern, E. Berg, P. Jarillo-Herrero, and S. Ilani, Nature **582**, 203 (2020).
- <sup>41</sup> D. Wong, K. P. Nuckolls, M. Oh, B. Lian, Y. Xie, S. Jeon, K. Watanabe, T. Taniguchi, B. A. Bernevig, and A. Yazdani, Nature **582**, 198 (2020).
- <sup>42</sup> M. He, Y. Li, J. Cai, Y. Liu, K. Watanabe, T. Taniguchi, X. Xu, and M. Yankowitz, Nature Physics **17**, 26 (2021).
- <sup>43</sup> A more direct evidence of symmetry breaking has been also found at three-quarter filling of the lowest conduction band, where a clear signal of ferromagnetism has been observed.
- <sup>44</sup> The deviation of the Fermi line with respect to the three extended saddle points shown in the figure remains within a few tenths of meV.
- <sup>45</sup> A. L. Fetter and J. D. Walecka, *Quantum Theory of Many-Particle Systems* (McGraw-Hill, New York, 1971).
- <sup>46</sup> L. P. Gor'kov and E. I. Rashba, Phys. Rev. Lett. **87**, 037004 (2001).
- <sup>47</sup> P. Moon and M. Koshino, Phys. Rev. B **87**, 205404 (2013).
- <sup>48</sup> A. N. Kolmogorov and V. H. Crespi, Phys. Rev. Lett. **85**, 4727 (2000).
- <sup>49</sup> A. N. Kolmogorov and V. H. Crespi, Phys. Rev. B **71**, 235415 (2005).
- <sup>50</sup> A. V. Maharaj, I. Esterlis, Y. Zhang, B. J. Ramshaw, and S. A. Kivelson, Phys. Rev. B **96**, 045132 (2017).
- <sup>51</sup> N. W. Ashcroft and N. D. Mermin, *Solid State Physics* (Saunders College Publishing, 1976).